SHELL-SIDE FLOW STUDY AND STRUCTURAL OPTIMIZATION OF A DOUBLE HELICAL-LIKE FLOW HEAT EXCHANGER

by

Xin GU[a], Wei GAO[a], Menghong LI[a], Qiming SHI[a], and Kan CAO[b*]

[a] School of Mechanical and Power Engineering, Zhengzhou University, Zhengzhou, China
[b] School of Energy and Environment, Zhongyuan University of Technology, Zhengzhou, China

Original scientific paper
https://doi.org/10.2298/TSCI220521133G

A double helical-like flow heat exchanger model was built, its shell-side flow state was studied by the CFD method, and the difference in heat transfer performance between it and the torsional flow heat exchanger was compared. From the numerical simulation results, it is found that the heat transfer coefficient and pressure drop are improved by 7.07-8.93% and 15.50-18.22%, respectively at the same flow rate, and the comprehensive performance expressed as $Nu/f^{1/3}$ is improved by 21.84-24.08%. Using the orthogonal test method to optimize the shell-side structure, it is found that the comprehensive performance is influenced by the two factors of spacing/groups and angle of baffles, and the influence of the deflection angle of two adjacent groups of baffles is very small, and the optimal structural combination of comprehensive performance is 30-0-70/11 (the angle of baffles is 30°, the deflection angle of two adjacent groups of baffles is 0°, the spacing between two adjacent sets of baffles is 70 mm, and the number of baffle groups is 11). The reliability and feasibility of the simulation method were verified by experiments.

Key words: *double helical-like flow, CFD, structural optimization, orthogonal test*

Introduction

As one of the most common equipment in industrial production, heat exchangers play a key role in many fields such as petroleum, HVAC, aviation, chemical, nuclear power, food, and pharmaceuticals, and especially have a very important position in petroleum refining and chemical processing [1, 2]. With the emphasis on resource conservation and environmental protection, the requirement for high efficiency heat exchangers is also increasing [3].

The shell-and-tube heat exchangers (STHX), which are more frequently used in the process industry, are widely used in chemical production because of their simple structure, easy processing, high pressure resistance, and wide range of applications [4, 5]. Tube-side strengthening and shell-side strengthening can improve the performance of STHX from different perspectives, while the main method of shell-side strengthening is the improvement and optimization of the baffle structure. For example, structures such as Rod Baffles [6, 7], Branch Baffles [8], Louvre Baffles [9, 10], and Flower Baffles [11, 12] are used to enhance the heat transfer performance and reduce the shell-side flow resistance by giving a specific flow state to the fluid. Lutcha *et al.* [13] developed a helical baffle heat exchanger (HBHX) in the 1990's, which mainly has the following advantages: there is basically no flow dead zone, small pressure drop loss,

* Corresponding author, e-mail: caokan96@163.com

and low power consumption, and it can effectively reduce the accumulation of fouling deposits on the shell-side and improve the life cycle of the heat exchangers [14]. Due to the difficulty of processing continuous helical baffle, the discontinuous baffle structure is mainly studied and applied at present. The use of a fan or elliptical plane lap to form a helical-like surface structure so that the shell-side fluid presents a helical flow state. Lei *et al.* [15] studied HBHX with different helix angles and found that the Nusselt number has the same trend as the helix angle at helix angles less than 30°, while the opposite is true at angles greater than 30°. Compared with the segmented baffle heat exchanger (SBHX), the HBHX has a lower Δp (pressure drop on the shell-side) with the same h (heat transfer coefficient). Dong *et al.* [16] studied the flow and heat transfer performance of a three-stage HBHX with different circumferential overlap sizes and showed that the plan with a triangular region covering two rows of tubes (20° T2CO) was superior with the highest Nusslet number and a comprehensive index and the strongest secondary flow. Hou *et al.* [17] proposed a new type of stepped HBHX, whose shell-side fluid-flows in a nearly helical shape with a more uniform velocity distribution and better comprehensive performance than the SBHX, while better solving the problem of leakage between adjacent baffles.

Improving the h as much as possible, reducing the Δp on the shell side, and improving the comprehensive performance factor related to both h and Δp are the main means to improve the performance of the heat exchanger. The lateral flow of the fluid on the shell-side of the heat exchanger can better flush the tube bundle to enhance the heat exchange effect, while the longitudinal flow of the fluid can reduce the flow resistance and reduce the pressure drop on the shell-side.The shell-side flow of various helical flow heat exchangers combines the characteristics of longitudinal flow well, but the heat transfer coefficient is not ideal compared with traditional heat exchangers such as SBHX. Considering the comprehensive performance of the heat exchanger, taking into account the heat transfer and pressure drop is a feasible research direction. The torsional flow heat exchanger (TFHX) [18] is a new type of heat exchanger developed by comprehensively utilizing the advantages of both, which shell-side fluid obliquely flush the tube bundle and presents a periodic twisted flow state. Based on the idea of oblique flow, a kind of double helical-like flow heat exchanger (DHLFHX) is proposed in this paper. The shell-side is two helical-like flows that are entangled with each other. The arrangement of baffles is similar to that of TFHX. Different from the co-directional arrangement of the baffles of the TFHX, the baffles in each baffle group of the DHLFHX are arranged symmetrically and inclined at the same angle to guide the fluid on the shell-side to flow obliquely and form a double helix shape. A comparative study of the shell-side flow state and heat transfer performance of the DHLFHX and the TFHX was carried out.Through the performance of these two heat exchangers in terms of h and Δp, the influence and effect of helical flow and oblique flow on the comprehensive performance are explored, which can provide some reference for the study of shell-side flow state of helical flow heat exchanger and the development of new support structure.

Models and method

Models

The overall models of the TFHX and DHLFHX are shown in fig. 1. The shell-side structure of the TFHX consists of multiple trapezoidal-like baffles arranged in parallel as a group, with two adjacent groups arranged vertically along the tube length direction with equal spacing. The shell-side structure of the DHLFHX is composed of two semi-elliptical baffles which cross relatively at a certain angle and an array of baffles arranged at a certain distance.

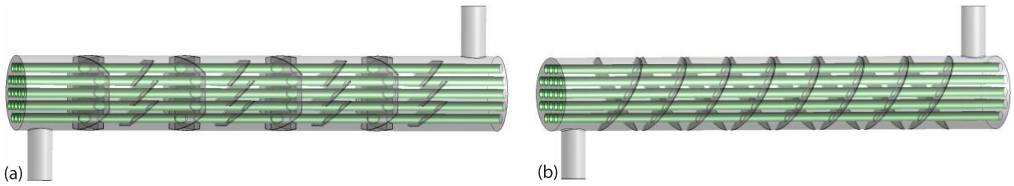

Figure 1. Overall models of heat exchangers; (a) TFHX and (b) DHLFHX

Figure 2 shows the tubes and baffles arrangement of the two heat exchangers, and other parameters are shown in tab. 1.

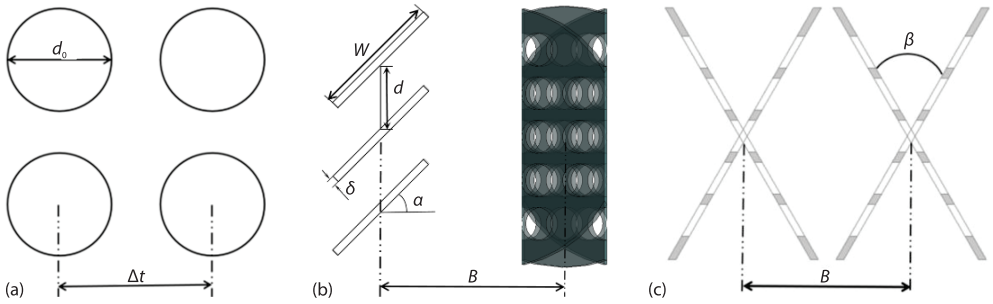

Figure. 2 Arrangement of tubes and baffles; (a) tube arrangement, (b) trapezoidal inclined baffle, and (c) semi elliptical baffle

Tabela 1. Parameter of heat exchanger model

Parameter	TFHX	DHLFHX
Inner diameter of cylinder, D [mm]	150	150
Inner diameter of inlet and outlet, d [mm]	50	50
Length of heat exchange tube, l [mm]	1000	1000
Outer diameter of tube, d_0 [mm]	19	19
Tube spacing, Δt [mm]	25	25
The thickness of baffle, δ [mm]	4	4
Transverse spacing of baffle, B [mm]	100	100
Longitudinal spacing of baffle, p [mm]	40	–
Width of baffle, W [mm]	70	–
Length of the short axis, a [mm]	–	75
Angle of inclination, α [°]	45	–
Angle of baffles, β [°]	–	60

Meshing and boundary conditions

The unstructured grid is used to mesh the fluid region of the DHLFHX, and the grid independence is verified by gradually reducing the grid size when Reynolds number is 4000. As shown in fig. 3, when the number of grids increases to about 6.52 million, the calculated results of performance parameters basically stabilize, and the difference with the calculated results under 7.21 million grids is around 1%. The calculation accuracy is shown in tab. 2 and

the grid schematic is shown in fig. 4. The maximum value of grid skewness is 0.83627 and the average value is 0.22002.

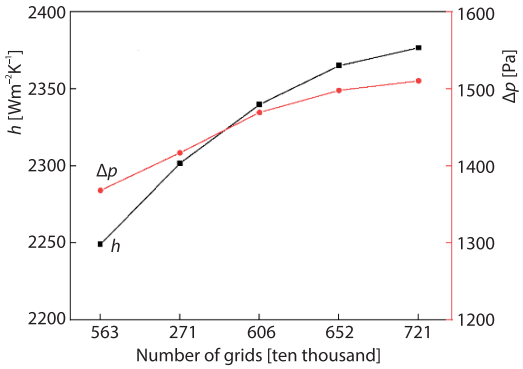

Figure 3. The trends of h and Δp with grids

Figure 4. Mesh geometry

Table 2. Calculation accuracy

Number of grids [ten thousand]	h [Wm^{-2}K^{-1}]	Deviation	Δp [Pa]	Deviation
563	2248.98	–	1368.22	–
571	2301.74	2.29%	1417.02	3.44%
606	2339.83	1.63%	1459.33	2.90%
652	2365.05	1.07%	1498.09	2.58%
721	2376.69	0.49%	1510.42	0.81%

The various types of boundary conditions and calculation methods such as coupling method, discrete format, and turbulence model used in the calculation are shown in tab. 3 [19, 20].

Table 3. Methods/boundary conditions

Items	Methods/conditions
Pressure-velocity coupling	SIMPLE
Discrete format	Second-order upwind (momentum, energy)
Turbulence model	Realizable k-ε (DHLFHX), RNG k-ε (TFHX)
Inlet and outlet	Velocity inlet, water, 293.15 [K], pressure outlet, zero external pressure, viscosity term 5%, hydraulic diameter 50 [mm]
Tubes	Assuming constant wall temperature, temperature 393.15 [K]
Walls (shell inner wall,baffle walls)	Adiabatic, non-slip boundary conditions

Governing equations

The governing equations in the computational domain of both heat exchangers [21]:

– Continuity equation

$$\frac{\partial}{\partial x_i}\left(\rho u_i\right) = 0 \tag{1}$$

– Momentum equati

$$\frac{\partial}{\partial x_j}\left(\rho u_i u_j\right) = -\frac{\partial p}{\partial x_i} + \frac{\partial p}{\partial x_j}\left(\mu\frac{\partial u_i}{\partial u_j} - \overline{\rho u_i' u_j'}\right) + S_i \tag{2}$$

– Energy equation:

$$\frac{\partial}{\partial x_j}\left[u_j\left(\rho E + p\right)\right] + \nabla\left[U\left(\rho E + p\right)\right] = \frac{\partial}{\partial x_j}\left[\lambda_{\text{eff}}\frac{\partial T}{\partial x_j} - u_i\left(\tau_{ij}\right)_{\text{eff}}\right] + S_h \tag{3}$$

Result analysis and structure optimization

Shell-side flow analysis

The shell-side streamline-velocity vector of the two heat exchangers at the flow rate of 2.01 kg/s is shown in fig. 5. For the DHLFHX, the fluid begins to twist and disperse from the first group of baffles into two quasi helical flows which are intertwined with each other after entering the shell-side zone. As seen in fig. 5(a), the fluid in flow Channel 1 and flow Channel 2 can be basically regarded as two helical flows of the same pitch. The velocity of the fluid increases as it crosses the angle between the baffles, while between two adjacent sets of baffles, the fluid velocity decreases again due to the increased flow channel, so the fluid will form an acceleration and deceleration cross between the groups of baffles, and the turbulence intensity of the fluid is enhanced, which can achieve the purpose of thinning the boundary-layer to strengthen heat transfer. For the TFHX, the shell-side fluid increases in velocity and turbulence intensity as the flow channel becomes smaller when passing through the baffles, but a large low flow velocity zone is formed in the backside of the baffles, the Zone B in fig. 5(b), which hurts heat transfer.

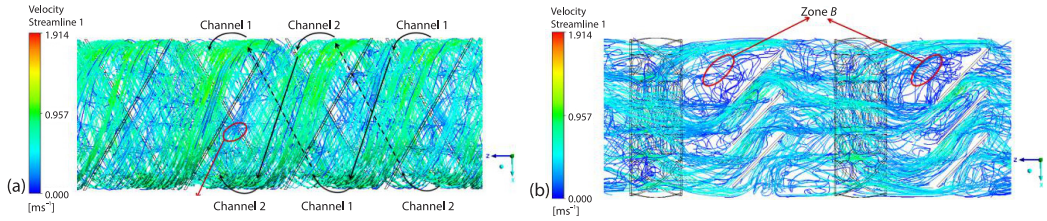

Figure 5. Streamline-velocity vector of the shell-side fluid; (a) DHLFHX and (b) TFHX

Figure 6 shows the velocity clouds of the transverse section of the two heat exchangers at Z = 450 mm (the middle radial section of the fourth set of baffles) at the flow rate of 2.01 kg/s. As seen from fig. 6(a), the fluid velocity distribution of the DHLFHX basically shows a gradual decrease from the outside to the inside, and the low velocity zone is less than the torsional flow heat exchanger and is basically concentrated near the symmetrical tubes on both sides, which are located in Zones A_1 and A_2 in fig. 6(a) (A_1 and A_2 are the symmetric areas of the two channels, and corresponding to the Zone A in fig. 5(a)). Because the fluid crosses the corner of the baffles and cannot touch the same direction downstream baffle in time, resulting in the decrease of fluid velocity in Zone A. Because of the orthogonal arrangement of the adjacent two groups of baffles of the TFHX, the overall shell-side fluid shows a periodic torsional flow state. The fluid-flow velocity between the central baffle is higher due to the guide effect of the baffles, and the fluid turbulence intensity is stronger, which helps to strengthen the heat transfer, but there is a large low velocity zone on the backside of the baffles near the wall, as shown in Zone B of fig. 6(b), corresponding to the Zone B in fig. 5(b).

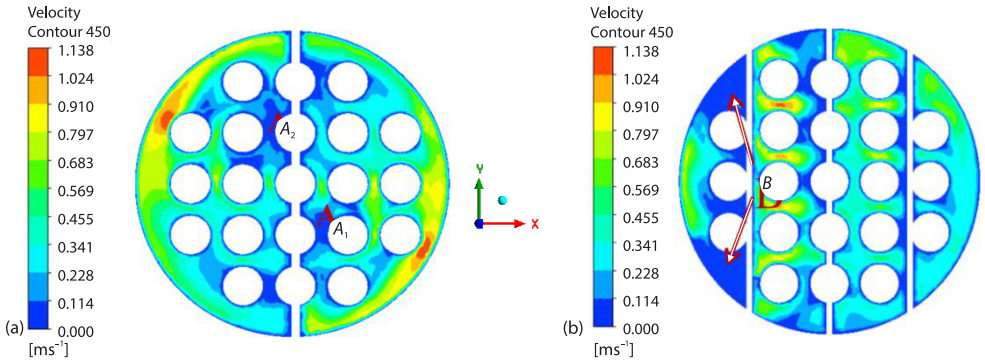

Figure 6. Clouds of transverse section velocity of shell-side; (a) DHLFHX and (b) TFHX

Figure 7 shows the temperature distributions of the DHLFHX and the TFHX at $Z = 650$ mm and 850 mm sections (the middle radial section of the 6th and 8th sets of baffles) at the flow rate of 2.01 kg/s. From the temperature distribution of the two cross-sections, it can be seen that the DHLFHX has better temperature distribution uniformity than the TFHX at the same cross-section, and the average temperature value in the same cross-section is also higher, indicating that the DHLFHX has a better heat transfer performance.

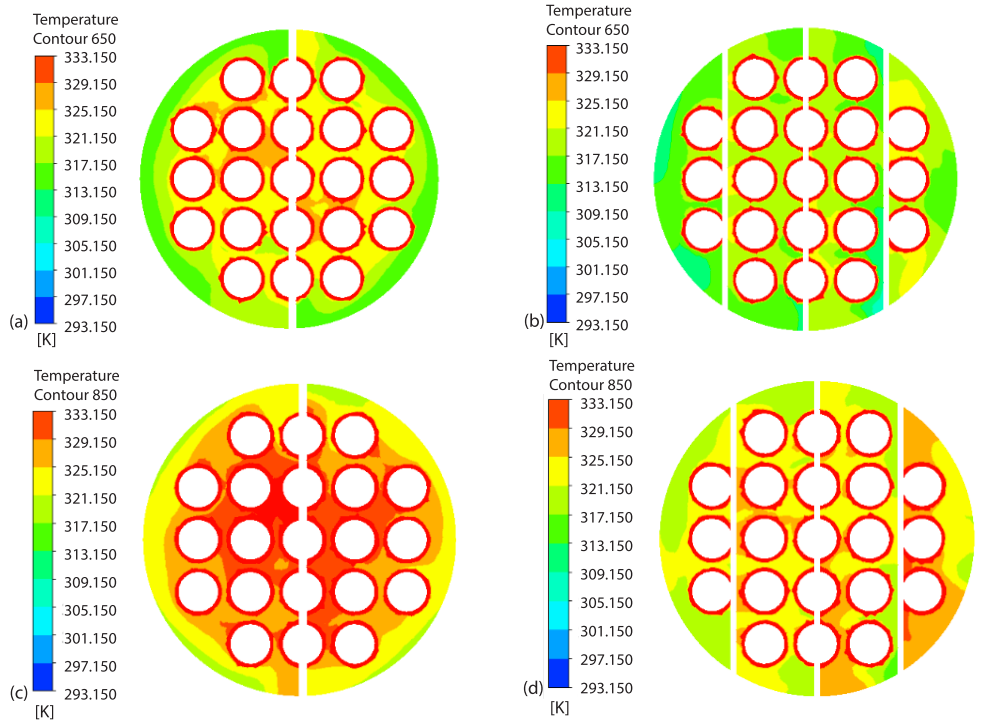

Figure 7. Temperature distribution in different sections; (a) DHLFHX $Z = 650$ mm, (b) TFHX $Z = 650$ mm, (c) DHLFHX $Z = 850$ mm, and (d) TFHX $Z = 850$ mm

Shell-side h, Δp, and comprehensive performance

Figures 8 and 9 show the trends of h and Δp with the mass-flow rate of the TFHX and the DHLFHX. As can be seen from the figures, the h and Δp of both heat exchangers increase with increasing mass-flow rate, and the h and Δp of the DHLFHX are higher than those of the TFHX at the same flow rate. From the calculation results, the h of the DHLFHX is increased by 7.07-8.93% and the Δp is increased by 15.50-18.22% compared with the TFHX. Since the shell-side fluid of the TFHX better combines the characteristics of longitudinal flow, the flow resistance on the shell-side is significantly reduced, so the Δp on the shell-side is also lower relative to the DHLFHX

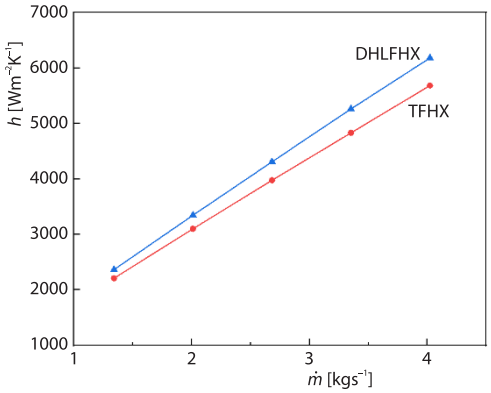

Figure 8. Trend of h with flow rate

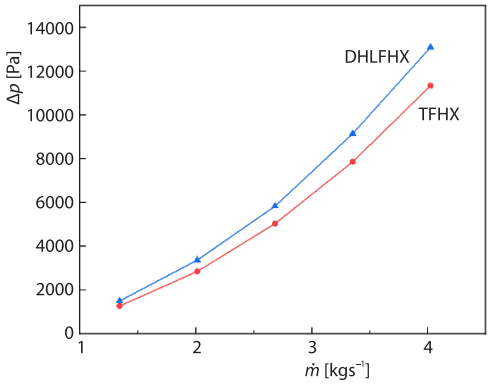

Figure 9. Trend of Δ*p* with flow rate

From a single result, the DHLFHX has an advantage in terms of h, while the TFHX also has an advantage in terms of shell-side Δp. To evaluate the shell-side enhanced heat transfer performance more uniformly, the comprehensive evaluation factor η [22, 23] was utilized to measure the comprehensive performance of the DHLFHX and the TFHX. The specific expression:

$$h = \frac{\dot{m}c_p\left(t_{\text{out}} - t_{\text{in}}\right)}{A\Delta t_m} \tag{4}$$

$$\text{Nu} = \frac{hd_0}{\lambda} \tag{5}$$

$$f = \frac{2d_0\Delta p}{l\rho u^2} \tag{6}$$

$$\eta = \frac{\text{Nu}}{f^{1/3}} \tag{7}$$

A comparison of the comprehensive performance results of the DHLFHX and TFHX is shown in fig. 10, it is calculated that the DHLFHX improves the comprehensive performance by 21.84-24.08% compared to the TFHX. Due to the difference of the shell-side structure, the characteristic velocity of the fluid on the shell-side of the DHLFHX is larger (the characteristic velocity is the maximum velocity of the fluid sweeping the tube bundle, and the average velocity of the minimum cross-sectional area of the fluid-flowing through the shell-side is taken as the characteristic velocity), so under the same mass-flow rate, the turbulence on the shell-side

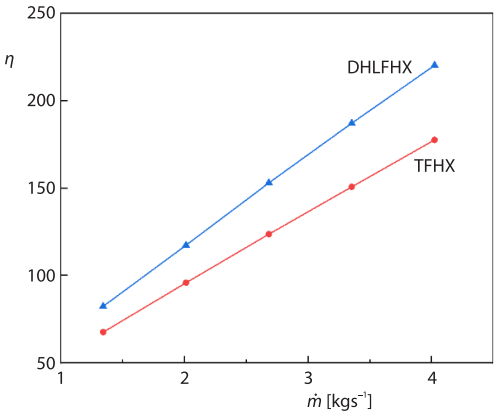

Figure 10. Trend of η with flow rate

of the DHLFHX is stronger, the increase in heat transfer coefficient brings greater benefits and the heat transfer effect is better.

Orthogonal test optimization

Orthogonal test design

The orthogonal test is a research method to analyze the situation for multiple factors and levels. Based on orthogonality select some points with representative levels from the overall test, which greatly reduces the number of tests and blindness, and has the advantages of high efficiency, rapidity, and economy [24]. To design the orthogonal test, three parameters of Angle of baffles, spacing/groups, and deflection angle of two adjacent groups of baffles were used as factors, and three levels of each factor were set to design the orthogonal test, and L9(3^3) orthogonal test table was selected for analysis and simulated at the flow rate of 2.01 kg/s. The orthogonal test factors and levels table and simulation results are shown in tabs. 4 and 5.

Table 4. Factors and levels

Levels	Factors		
	Angle of baffles [°]	Deflection angle [°]	Spacing/groups [mmn^{-1}]
1	30	0	140/6
2	45	45	100/8
3	60	90	70/11

Table 5. Simulation results

Angle of baffles [°]	Deflection angle [°]	Spacing/groups [mmn^{-1}]	h [Wm^{-2}K^{-1}]	Δp [Pa]	η
30	0	140-6	4393.64	12031.80	123.94
30	45	100-8	4567.64	12858.90	129.75
30	90	70-11	5076.37	17736.81	140.82
45	0	100-8	3946.61	6043.84	128.32
45	45	70-11	4116.58	6581.10	132.24
45	90	140-6	3649.41	5272.93	118.30
60	0	70-11	3778.91	4144.96	132.64
60	45	140-6	3158.52	2979.91	111.15
60	90	100-8	3327.71	3443.76	115.09

Result analysis

The simulation results were analyzed by using the extreme difference analysis method. By calculating the average values of different levels of the same test factors, and finding

the difference of the average value in the same group of data, the larger the difference value indicates the greater the influence of the factors on the objective function, and the degree of influence of the parameters on the objective function can be derived by ranking the different size. The effects of the levels of the factors on the h, Δp, and η are shown in tabs. 6-8.

Table 6. Effect of factors and levels on *h*

Levels	h [Wm^{-2}K^{-1}]		
	Angle of baffles [°]	Deflection angle [°]	Spacing/groups [mmn^{-1}]
Average value 1	4679.21	4039.72	3733.85
Average value 2	3904.2	3947.58	3947.32
Average value 3	3422.05	4017.83	4323.95
Extreme Difference	1279.16	21.89	590.1
Degree of influence	Angle of baffles > Spacin/groups > Deflection angle		
A maximum combination of h	30-0-70/11		

Table 7. Effect of factors and levels on Δp

Levels	Δp [Pa]		
	Angle of baffles [°]	Deflection angle [°]	Spacing/groups [mmn^{-1}]
Average value 1	14209.16	7406.87	6761.54
Average value 2	5967.29	7474.64	7448.83
Average value 3	3522.87	8817.83	9488.95
Extreme difference	10686.29	1410.96	2727.41
Degree of influence	Angle of baffles > Spacing/groups > Deflection angle		
A minimum combination of Δp	60-0-140/6		

Table 8. Effect of factors and levels on η

Levels	η		
	Angle of baffles [°]	Deflection angle [°]	Spacing/groups [mmn^{-1}]
Average value 1	131.50	128.30	117.78
Average value 2	126.29	124.38	124.39
Average value 3	119.62	124.74	135.23
Extreme Difference	11.88	3.92	17.45
Degree of influence	Spacing/groups > Angle of baffles > Deflection angle		
A maximum combination of η	30-0-70/11		

The analysis of the results from tabs. 6-8 shows that for the h and Δp, the degree of influence is angle of baffles > spacing/groups > deflection angle, the angle of baffles is the main influence factor and deflection angle is the most minor influence factor. For the η, the degree of influence spacing/groups > angle of baffles > deflection angle, the spacing/groups is the main influence factor and the deflection angle is the most minor influence factor. Considering only the index of minimum pressure drop, the best combination is 60-0-140/60, and after modelling, the minimum pressure drop is 2934.17 [Pa]. Considering the h and η, the best combination is 30-0-70/11, and the highest h is 5097.51 W/m^{2}K, and the highest η is 141.76, which is 20.78% higher than the initial structure.

Experimental verifications

The shell-side fluid-flow velocity of the TFHX model was measured using LDV equipment, and the tracer particles were captured using a laser Doppler velocimeter and processed by Flowsizer software to obtain the velocity values at the measured locations. The experimental instrumentation is summarized in tab. 9, and the model is shown in fig. 11.

Table 9. Experimental instruments

Name	Specification/model
Rotameter	Model LZB-50, precision 2.0 grade
Submersible pump	Model MJ-NS6500, maximum head 3.5 [m]
Tracer particle	Model 10089 (spherical), density 0.00105-0.00115 [kgm^{-3}]

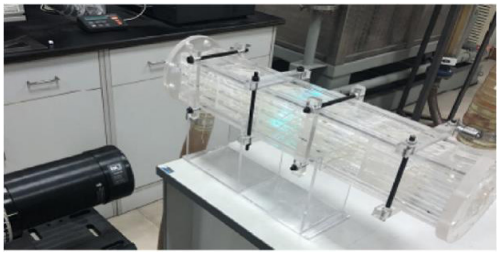

Figure 11. Experimental model

The midpoint of two adjacent sets of baffles is selected as the measurement point on the validation-line, and the longitudinal velocity components (velocity components parallel to the heat exchanger tube direction) and transverse velocity components (velocity components perpendicular to the heat exchanger tube direction) were measured and compared with the velocity components of the simulation results. Figure 11 shows the degree of coincidence of the velocity components.

As can be seen from fig. 12, the TFHX shell-side fluid has significant periodic flow characteristics, and the simulated values of transverse velocity and longitudinal velocity compared to the experimental value of the maximum relative error of about 18% do not exceed the allowable range, the experiment verified the reliability and feasibility of the numerical simulation method. The reasons for the errors are the tube box, flange, inlet, and outlet receiver structures are not considered; ignoring the gap between the baffles and the tube bundle.; there are errors in the model processing and manufacturing, *etc.*

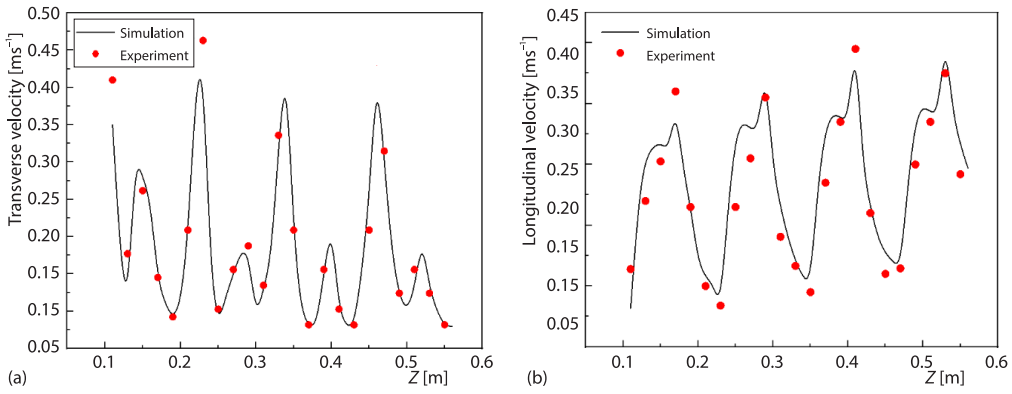

Figure 12. Comparison of velocity components; (a) transverse velocity and (b) longitudinal velocity

Conclusions

- For the DHLFHX, after entering the shell-side and passing through the first group of baffles, the fluid will be twisted and dispersed into two helical-like flows which are intertwined with each other. The fluid will accelerate and decelerate between the adjacent baffle groups, which increases the turbulence intensity and plays a positive role in promoting the heat exchange performance. Compared with the TFHX, the DHLFHX has better temperature distribution uniformity and higher average temperature values in the same cross-section.
- At the same mass-flow rate, the h of the DHLFHX is increased by 7.07-8.93% compared to the TFHX, but the comprehensive performance η expressed as $Nu/f^{1/3}$ is increased by 21.84-24.08%, because under the influence of the shell side structure, the shell characteristic velocity has been increased, so the shell side Reynolds number is larger and the turbulence degree is stronger under the same mass-flow rate, which has a significant effect on the enhancement of heat transfer performance.
- Using the orthogonal test method to optimize the shell-side structure of the DHLFHX at the flow rate of 2.01 kg/s. Within the scope of this paper, it was found that the h and the η were most sensitive to the changes in the spacing/groups and the angle of baffles, and a smaller baffle spacing and angle of baffles arrangement could significantly improve the comprehensive performance.
- The reliability and feasibility of the numerical simulation method were verified by comparing the measurement of the velocity components on the shell side of the TFHX and the degree of velocity compliance.

Nomenclature

a – length of the short axis, [mm]
A – heat exchange surface area, [m^2]
B – transverse spacing of baffle, [mm]
c_p – specific heat capacity, [$Jkg^{-1}K^{-1}$]
D – inner diameter of the cylinder, [mm]
d – inner diameter of inlet and outlet, [mm]
d_0 – outer diameter of the tube, [mm]
f – friction factor, [–]
h – heat transfer coefficient, [$Wm^{-2}K^{-1}$]
l – length of heat exchange tube, [mm]
$\dot{m}$ – mass-flow rate, [kgs^{-1}]
Nu – Nusselt number, [–]
p – longitudinal spacing of baffle, [mm]
Δp – pressure drop, [Pa]
Re – Reynolds number, [–]
t_{out} – outlet fluid temperature, [K]
t_{in} – inlet fluid temperature, [K]
Δt – tube spacing, [mm]
Δt_m – log-mean temperature difference, [K]
u – fluid velocity, [ms^{-1}]
W – baffle width, [mm]

Greek symbols

α – angle of inclination, [°]
β – angle of baffles, [°]
η – comprehensive evaluation factor, [–]
ρ – density, [kgm^{-3}]
λ – thermal conductivity, [$Wm^{-1}K^{-1}$]
δ – baffle thickness, [mm]

References

[1] Wang, Q., *et a*l., Review of Improvements on Shell-and-Tube Heat Exchangers with Helical Baffles, *Heat Transfer Engineering*, *31* (2010), 10, pp. 836-853
[2] Thome, J. R., A Review on Shell-and-Tube Heat Exchangers for the Chemical Processing Industry: Heat Transfer Augmentation, *Journal Enhanc Heat Transf*., *24* (2017), 1-6, pp. 427-441
[3] Arani, A. A. A., Moradi R., Shell and Tube Heat Exchanger Optimization Using New Baffle and Tube Configuration, *Applied Thermal Engineering*, *157* (2019), 113736
[4] Farajollahi, B., *et al*., Heat Transfer of Nanofluids in a Shell and Tube Heat Exchanger, *International Journal of Heat and Mass Transfer*, *53* (2010), 1-3, pp. 12-17
[5] Zhang, X., *et al.*, Numerical Simulation on a Novel Shell-and-Tube Heat Exchanger with Screw Cinquefoil Orifice Baffles, *Advances in Mechanical Engineering*, *9* (2017), 8

[6] Ma, L., *et al*., Analysis of Flow and Heat Transfer in Rod Baffle Heat Exchangers with Rods of Variable Sections, *Journal of Engineering Thermophysics*, *33* (2012), 1, pp. 113-116
[7] Yuanzhe, C., *et al*., Performance Comparison of Rod-Baffle and Segment-Baffle Heat Exchangers Using Numerical Simulations, *Applied Mechanics and Materials*, *595* (2014), July, pp. 128-133
[8] Wang, K., *et al*., Fluid-Flow and Heat Transfer Characteristics Investigation in the Shell Side of the Branch Baffle Heat Exchanger, *Journal of Applied Fluid Mechanics*, *14* (2021), 6, pp. 1775-1786
[9] Lai, H., Numerical Study of Flow and Heat Transfer of Heat Exchanger with Louver Baffles, *Applied Mechanics and Materials*, *721* (2014), Dec., pp.174-177
[10] Lei, Y., *et al*., Design and Performance Analysis of the Novel Shell-and-Tube Heat Exchangers with Louver Baffles, *Applied Thermal Engineering*, *125* (2017), Oct., pp. 870-879
[11] Chen, J., *et al*., Experimental Investigation of Shell-Side Performance and Optimal Design of Shell-and-Tube Heat Exchanger with Different Flower Baffles, *Heat Transfer Engineering*, *42* (2021), 7, pp. 613-626
[12] Sahel D., Thermal Performance Assessment of a Tubular Heat Exchanger Fitted with Flower Baffles, *Journal of Thermophysics and Heat Transfer*, *35* (2021), 4, pp. 726-734
[13] Lutcha, J., Nemcansky J., Performance Improvement of Tubular Heat-Exchangers by Helical Baffles, *Chemical Engineering Research and Design*, *68* (1990), 3, pp. 263-270
[14] Salahuddin, U., *et al*., A Review of the Advancements Made in Helical Baffles Used in Shell and Tube Heat Exchangers, *International Communications in Heat and Mass Transfer*, *67* (2015), Oct., pp. 104-108
[15] Lei, Y.-G., *et al*., Effects of Baffle Inclination Angle on Flow and Heat Transfer of a Heat Exchanger with Helical Baffles, *Chemical Engineering and Processing-Process Intensification*, *47* (2008), 12, pp. 2336-2345
[16] Dong, C., *et al*., Performance Comparison of Trisection Helical Baffle Heat Exchangers with Different Circumferential Overlap Sizes, *Chemical Engineering and Technology, 38* (2015), 7, pp. 1277-1284
[17] Hou, L., *et al*., Study on Flow and Heat Transfer Characteristics of the Heat Exchanger with Stepped Helical Baffles, *Journal of Engineering Thermophysics*, *39* (2018), 11, pp. 2498-2502
[18] Gu, X., *et al*., Characteristics of Fluid-Flow and Heat Transfer in the Shell Side of the Trapezoidal-Like Tilted Baffles Heat Exchanger, *Journal of Thermal Science*, *27* (2018), 6, pp. 602-610
[19] Yang, D., *et al*., Geometric Optimization of Shell and Tube Heat Exchanger with Interstitial Twisted Tapes Outside the Tubes Applying CFD Techniques, *Applied Thermal Engineering*, *152* (2019), Apr., pp. 559-572
[20] Sun, Y., *et al*., Numerical Study of the Shell-Side Performance of the Trisection Baffled and Quartern Baffled Heat Exchangers, *Heat Transfer Research*, *45* (2014), 8, pp. 701-723
[21] Gu, X., *et al*., Multi-Objective Optimization on Structural Parameters of Torsional Flow Heat Exchanger, *Applied Thermal Engineering*, *161* (2019), 113831
[22] Tan X.-H., *et al*., Heat Transfer and Pressure Drop Performance of Twisted Oval Tube Heat Exchanger, *Applied Thermal Engineering*, *50* (2013), 1, pp. 374-383
[23] Li, X., *et al*., Applicability and Feasibility Study on the Evaluation Indexes of Heat Exchanger Energy Efficiency, *Journal of Engineering for Thermal Energy and Power*, *34* (2019), 2, pp. 137-144
[24] Jianhuang, H., *et al*., Numerical Simulation and Structure Optimization on the Corrugated Tubes of a Double Pipe Heat Exchanger, *Applied Mechanics and Materials*, *385-386* (2013), Aug., pp. 65-68

Paper submitted: May 21, 2022
Paper revised: August 15, 2022
Paper accepted: August 18, 2022